Available online at www.sciencedirect.com
ScienceDirect
Journal of Power Sources 172 (2007) 560–569
JOURNAL OF POWER SOURCES
www.elsevier.com/locate/jpowsour

# Enhancement of the electrooxidation of ethanol on Pt–Sn–P/C catalysts prepared by chemical deposition process

Xinzhong Xue [a,b], Junjie Ge [a,b], Tian Tian [a,b], Changpeng Liu [a], Wei Xing [a,*,1], Tianhong Lu [a]

[a] *Changchun Institute of Applied Chemistry, Chinese Academy of Science, Changchun 130022, PR China*
[b] *Graduate University of the Chinese Academy of Sciences, Beijing 100049, PR China*

Received 20 April 2007; received in revised form 15 May 2007; accepted 17 May 2007
Available online 26 May 2007

**Abstract**

In this paper, five $Pt_3Sn_1$/C catalysts have been prepared using three different methods. It was found that phosphorus deposited on the surface of carbon with Pt and Sn when sodium hypophosphite was used as reducing agent by optimization of synthetic conditions such as pH in the synthetic solution and temperature. The deposition of phosphorus should be effective on the size reduction and markedly reduces PtSn nanoparticle size, and raise electrochemical active surface (EAS) area of catalyst and improve the catalytic performance. TEM images show PtSnP nanoparticles are highly dispersed on the carbon surface with average diameters of 2 nm. The optimum composition is $Pt_3Sn_1P_2$/C (note PtSn/C-3) catalyst in my work. With this composition, it shows very high activity for the electrooxidation of ethanol and exhibit enhanced performance compared with other two $Pt_3Sn_1$/C catalysts that prepared using ethylene glycol reduction method (note PtSn/C-EG) and borohydride reduction method (note PtSn/-B). The maximum power densities of direct ethanol fuel cell (DEFC) were 61 mW $cm^{-2}$ that is 150 and 170% higher than that of the PtSn/C-EG and PtSn/C-B catalyst.


*Keywords:* Phosphorus; Hypophosphite; PtSnP nanoparticle; Eletrooxidation; Direct ethanol fuel cell (DEFC)

## 1. Introduction

Direct alcohol fuel cells (DAFCs) were attracting increasing interest as a compact power sources for portable applications, mainly due to the relatively simple handling, storage, and transportation of the fuel. Though the interests is focused on the use of methanol because of its better reaction kinetics and hence better performance in a fuel cell. However, the question of the toxicity of methanol remains crucial. Methanol is considered since a long time as a toxic product (mainly neurotoxic) [1]. It is to use other alcohols presenting negligible or very low chemical toxicity, which is essential, at least for some applications. Ethanol appears to be an interesting alternative fuel for a wide utilization. Its low toxicity added to its availability (from biomass products) is an important positive point for its use as an alternative fuel to methanol even if its reactivity is slightly lower. Hence, it is a promising liquid fuel for directly fueled DEFCs [1–7]. However, ethanol oxidation to $CO_2$ is associated with the cleavage of the C–C bond, which requires higher activation energy than C–H bond breaking, at least for currently known electrocatalysts [8–12]. To achieve this, it is necessary to modify the composition and structure of the anode catalyst [7,13–16].

The case of the oxidation of ethanol is more difficult than that of methanol with the necessity to break the C–C bond to obtain its complete oxidation. The reaction is known to proceed via a complex multistep mechanism, involving a number of adsorbed reaction intermediates and byproducts resulting from incomplete ethanol oxidation [17]. The major adsorbed intermediates were identified as adsorbed CO and C-1 and C-2 hydrocarbon residues, whereas acetaldehyde and acetic acid have been detected as the main byproducts using differential electrochemical mass spectrometry (DEMS), infrared spectroscopy, ion chromatography, and liquid chromatography [18–21]. Conversely to the case of methanol, Pt–Ru based electrocatalysts lead to poor improvement of the ethanol electrooxidation. Pt–Sn supported on high surface area carbon as the electrocatalysts of the anode for DEFCs is still considered

* Corresponding author. Tel.: +86 431 85262223; fax: +86 431 85685653.
*E-mail address:* xingwei@ciac.jl.cn (W. Xing).
[1] International Society of Electrochemistry Member.

0378-7753/$ – see front matter © 2007 Elsevier B.V. All rights reserved.
doi:10.1016/j.jpowsour.2007.05.091

to be the best catalysts among all those studied [1–16], and the $Pt_3Sn$ is one of the most active systems known for CO oxidation [22]. Lamy and co-workers have found that the Pt–Sn/C catalyst synthesized by impregnation–reduction method possessed much higher catalytic activity for ethanol electrooxidation than pure Pt [1,2,23,24]. Xin and co-workers also found PtSn catalysts prepared by modified polyol method showed superior performance for ethanol electro-oxidation [25,26]. DEFC testing data indicate high performance when either unsupported or supported Pt–Sn catalysts are used, depending on anode catalyst composition and particle size [1,2,4,7,25].

It has been reported that addition of a non-metallic element, P, drastically reduced the size of Fe single crystal in a magnetic alumite film [27]. Ultrafine amorphous alloy particles (UAAP) consisting of transition metal (M = Fe, Co, Ni) and metalloid element phosphorus have been studied extensively because of their interesting chemical and physical properties [28–31]. Many studies have addressed on the influences of P on the electronic state of metal elements, which obviously should have significant effects on some of the properties, e.g. magnetic and catalytic properties, of UAAP [31–34]. Okamoto et al. reported that a variation in 3d electron density on the nickel metal induced by phosphorus would modify the activity and selectivity of the nickel catalyst for hydrogenation [34]. Lukehart and co-workers [35] reported that they synthesized accidentally PtRuP2/C catalysts using five different Pt,Ru-bimetallic precursors as sources of metal. The results of experiment indicated that the presence of substantial amounts of PtRuP2 does not poison the catalytic performance of these catalysts and might even slightly enhance methanol electrooxidation. Daimon and Kurobe [36] studied that the addition of N, P and S reduced the size of PtRu catalyst particle deposited on carbon support and to improve the catalystic performance for methanol electrooxidation. In the previous work [37], we have also found that the PtRuP/C catalyst synthesized by hypophosphite deposition possessed much higher catalytic activity for methanol electrooxidation.

In this work, three kinds PtSnP/C catalysts and two kinds of $Pt_3Sn_1$/C electrocatalysts were prepared by different methods. It was found that deposited phosphorus can improve the dispersion of PtSn nanoparticles on carbon surface, reduce size of PtSn naoparticles and raise electrochemical active surface (EAS) area of catalyst when the sodium hypophosphite was used as reducing agent during the preparation of PtSn/C catalyst. The cyclic voltammetry and the single cell performance tests jointly show that $Pt_3Sn_1P_2$/C (PtSnP/C-3) catalysts present the highest activity for ethanol electrooxidation among five catalysts.

## 2. Experimental section

### 2.1. Catalyst preparation

#### 2.1.1. Materials

The chemical reagents $H_2PtCl_6{\cdot}6H_2O$ and $SnCl_2{\cdot}2H_2O$ were purchased from Aldrich Chemical Co. The sodium hypophosphite, sodium borohydride and sodium citrate were purchased from Beijing Chemical Co. The Vulcan Carbon powder XC-72 was purchased from Cabot Corporation. Ultrapure water (18.2 MΩ) was used to prepare the solutions. All solvents were reagent grade and used as received unless otherwise noted.

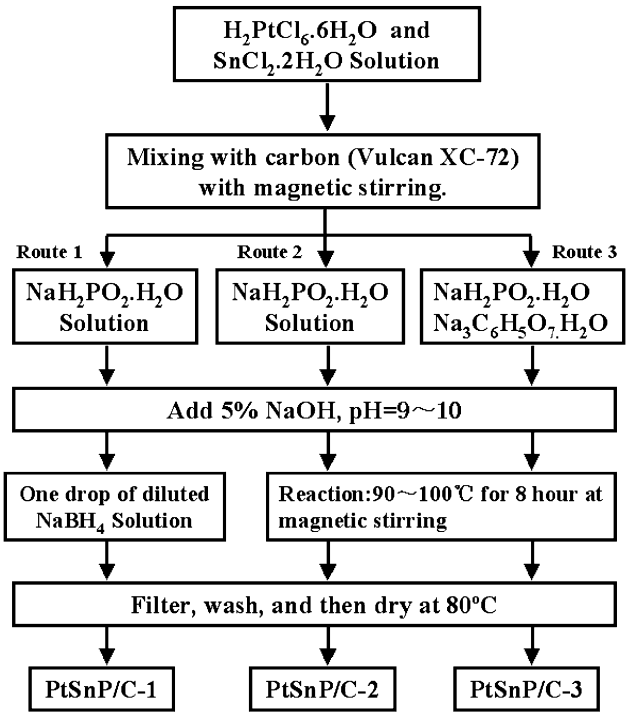


$$PtCl_6^{2-} + 2H_2PO_2^- + 2H_2O = 2H_2PO_3^- + 4H^+ + 6Cl^- + Pt \quad (1)$$

$$Sn^{2+} + H_2PO_2^- + H_2O = H_2PO_3^- + 2H^+ + Sn \quad (2)$$

$$3H_2PO_2^- = H_2PO_3^- + H_2O + 2OH^- + 2P \quad (3)$$

$$H_2PO_2^- + H_2O = H_2PO_3^- + H_2 \quad (4)$$

Fig. 1. Schematic flow chart of the preparation of carbon supported PtSnP electrocatalysts by the sodium hypophosphite method.

#### 2.1.2. Preparation of carbon supported PtSnP catalysts

We synthesized the catalyst using three routes, as shown in Fig. 1. The primary steps of this synthesis were given below: First, 165 mg $H_2PtCl_6{\cdot}6H_2O$ and 24 mg $SnCl_2{\cdot}2H_2O$ (the ratios of Pt:Sn = 3:1) aqueous solutions were mixed with 300 mg Vulcan XC-72 carbon in the distilled water. Then, the above solutions were ultrasonic agitation for 30 min in air at the room temperature. The appropriate amounts solution of sodium hypophosphite (1.35 g) and sodium citrate (125 mg) was then added into the mixture with stirring. The pH value of the solution was adjusted to 9.2 using a 5 wt% sodium hydroxide solution, subsequently heated to 90 °C for 8 h, and then cooled in air. The carbon-supported PtSnP catalysts were then filtered and extensively washed with distilled water. The carbon-supported PtSnP catalysts were generally dried at room temperature in air. The following four independent reactions may take place in the system during reduction of metal chlorides with sodium hypophosphite (see Fig. 1). This means that while the hypophosphite was used as reducing agent for the preparation of PtSn/C

alloy catalysts, the non-metallic phosphorus with platinum and tin deposited together on the surface of support. The PtSnP/C catalyst prepared by route 1, route 2 and route 3 were called as the PtSnP/C-1, PtSnP/C-2, PtSnP/C-3 catalysts, respectively.

#### 2.1.3. Preparation of carbon supported PtSn catalysts

For comparison, other two the total metal loading (Pt plus Sn) of 20 wt% PtSn/C catalysts were also synthesized by modified polyol method [25,26] and conventional reduction method.

Carbon supported PtSn catalyst was synthesized by modified polyol method. 165 mg $H_2PtCl_6{\cdot}6H_2O$ and 24 mg $SnCl_2{\cdot}2H_2O$ (the ratios of Pt:Sn = 3:1) were dissolved, respectively, in ethylene glycol or its mixture solution with water, in which the water volume content was 10%. Then following them, the pH of solution was modified to 12 and the temperature was increased up to 130 °C and kept constant for 2 h so that the metals were reduced adequately. Then the ultrasonically dispersed carbon slurry was added dropwise. After impregnation for 4 h, the mixture was filtered and the filter cake was dried in a vacuum oven at 80 °C for 2 h. The catalysts prepared in this way were called as PtSn/C-EG catalysts.

Impregnated Carbon supported PtSn catalyst was synthesized by the conventional reduction method. A 165 mg $H_2PtCl_6{\cdot}6H_2O$ and 24 mg $SnCl_2{\cdot}2H_2O$ (the ratios of Pt:Sn = 3:1) aqueous solutions were dispersed in a mixture of 250 mL deionized water. To this mixture, 300 mg Vulcan XC-72 carbon was added and the suspension was placed in an ultrasonic bath for 30 min. The suspension was stirred for 30 min before the pH was adjusted to 8.0 with 0.1 M $Na_2CO_3$ solution. The suspension continued stirring for complete impregnation. After that, reduction was performed by dropwise addition of 22 mL of 0.2 M $L^{-1}$ $NaBH_4$. The slurry was maintained at room temperature for 3 h to allow complete reduction of Pt and Sn. The slurry was filtered and washed copiously with hot distilled water to remove chloride ions. The catalyst was dried in vacuum oven at 80 °C for 2 h. The catalysts prepared in this way were called as PtSn/C-B catalysts.

The total metal loading (Pt plus Sn) was maintained at 20 wt%, for all the initial catalysts preparation in this work, and the Pt:Sn ratio of the precursor salts is 3:1.

### 2.2. Catalysts of physical characterization

The X-ray diffraction (XRD) patterns for the catalysts were obtained using a Rigaku-D/MAX-PC 2500 X-ray diffractometer with the Cu Kα (λ = 1.5405 Å) radiation source operating at 40 kV and 200 mA.

The bulk composition of the prepared catalysts and elements distribution were evaluated by energy dispersive X-ray analysis (EDX) in a scanning electron microscope (JEOL JAX-840).

The measurements of transmission electron microspectroscopy (TEM) were carried out with a JEOL 2010 microscope operating at 200 kV with nominal resolution. Samples were prepared by dispersing catalyst/ethanol suspension onto a 3-mm-diam copper grid covered with holey carbon film as a substrate, then evaporating the solvent and drying them in air.

X-ray photoelectron spectroscopy (XPS) was carried out using an ESCALAB MKII photoelectron spectrometer (VG Scientific). The fast entry chamber allowed rapid sample transfer from air to UHV pressures (base pressures during XPS analysis were in the low-to-mid $10^{-10}$ Torr range). The XPS experiments were performed in the spectroscopy chamber using a standard Mg anode X-ray source (and the Mg Kα X-rays at 1253.6 eV) and a 150 mm hemispherical electron energy analyzer.

### 2.3. Catalysts of electrochemical characterization

#### 2.3.1. Electrochemical measurement

An EG&G model 273A potentiostat/galvanostat (Princeton Applied Research) and a conventional three-electrode test cell were used for electrochemical measurements. A Pt flat was used as the counter electrode. The Ag/AgCl/$Cl^-$ electrode was used as the reference electrode. All the potentials were quoted with respect to the reference Ag/AgCl/$Cl^-$ electrode. The working electrode was a thin layer of Nafion impregnated catalyst cast on a glassy carbon disk held in a Teflon cylinder. The detailed preparation method was described in our previous work [38]. First, 5 mg of the Pt–Ru/C catalyst was dispersed ultrasonically in 1 mL of the alcohol solution with 50 μL of 5% Nafion solution. Then, 10 μL of the dispersion was pipetted and spread on a mirror-finished glassy carbon electrode with 3 mm diameter. Finally, the electrode was dried at room temperature for 30 min. The glassy carbon electrode was polished with slurry of 0.5 and 0.03 μm alumina successively and sonicated in the triple distilled water before use. The apparent surface area of the glassy carbon electrode was 0.07 $cm^2$. All electrolyte solutions were purged from the solution by bubbling with high purity nitrogen for 15 min prior to each electrochemical measurement. For cyclic voltammograms of ethanol were measured at the working electrode by cycling the potential between −0.2 and 0.9 V versus Ag/AgCl/$Cl^-$ at 10 mV $s^{-1}$ in the 0.5 M $H_2SO_4$ + 1 M $CH_3CH_2OH$ solution.

#### 2.3.2. Membrane electrode assembly (MEA) preparation and single DEFC testing

The membrane electrode assemble (MEA) was prepared as follows. The catalyst inks containing the appropriate weight percent of a Nafion solution (Aldrich) was spread on the surface of the carbon paper substrates (TGPH-090, E-Tek Co.) and formed the anode and cathode catalyst layers. Then, 160 μL of 5 wt% Nafion solution was spread on the catalyst layers and dried in the room temperature. The catalyst loadings based only on metal content were 1.5 mg $cm^{-2}$ of supported PtSn catalysts at the anode and 1.5 mg $cm^{-2}$ of 20 wt% Pt loadings on Vulcan XC-72 (E-TEK commercial catalyst) at the cathode. The MEA is fabricated by hot-pressing the anode and cathode catalyst layer onto the pretreated Nafion117 membrane for 2 min at 50 atm and 120 °C. To fabricate the single DEFC, the MEA is placed between two graphite current collectors with a serpentine design for the fuel and air distribution. The single cell was consisting of two ribbed graphite plates, which were compressed between two gold plated end stainless steel plates. These we provided with liquid and gas-feed tubes to which were connected the electric wires for the current/voltage measurements. To measure the performance of the single DEFC with a 3 cm × 3 cm active

cross-sectional catalyst area, and a fuel cell testing system (Arbin Instruments) that recorded cell potentials under constant-current conditions, A 2.0 M ethanol solution was preheated 70 °C and supplied to the anode with a 5.0 mL $min^{-1}$ flow rate and pure oxygen was fed to cathode with 100 mL $min^{-1}$ flow rate at 2 atm were used.

## 3. Results and discussion

Route 1: A drop of $NaBH_4$ solution is added to a mixture containing appropriate amounts of $H_2PtCl_6{\cdot}6H_2O$, 24 mg $SnCl_2{\cdot}2H_2O$ and $NaH_2PO_2{\cdot}H_2O$, which has a pH value of 9–10 adjusted by adding a sodium hydroxide solution, after an incubation period the autocatalytic reaction takes place at room temperature. And this explains the fact that heating was often needed to induce the reaction if there were no $NaBH_4$ added (route 2 and route 3). Moreover, based on mechanistic studies, the overall reaction of the production of PtSnP is suggested to be composed of the following four in dependent reactions. As shown in Fig. 1, the initial pH value of the solution was about 89–10. By adding a drop of $NaBH_4$ solution or heating the solution and after about 10 min incubation period, the pH value of the solution dropped rapidly because of the reduction of $PtCl_6^{2-}$ and $Sn^{2+}$ which produced $H^+$ as shown by Eqs. (1) and (2). When the pH value dropped to about 6–7, the reaction of Eq. (3) might slow down the decrease of pH value of the solution, and meanwhile large amounts of $H_2$ evolved due to the hydrolysis of $H_2PO_2^-$ as depicted by Eq. (4) catalyzed by the PtSnP/C-1, PtSnP/C-2, PtSnP/C-3 ultrafine alloy nanoparticles formed.

A summary of the preparation details and characterization data for each sample is provided in Table 1. The total metal and phosphorus content of each sample ranges from 10.50 wt% for sample PtSnP/C-1 to 19.68 wt% for PtSn/C-B catalyst, depending on different reducing conditions. Experimental results revealed that the different preparation conditions significantly affected the morphologies, particle sizes, surface area, and the concentration of phosphorus bonded to the platinum and tin metal. The compositions of these catalysts as determined by EDX were PtSnP/C-1 ($Pt_{1.57}Sn_{1.0}P_{1.33}$), PtSnP/C-2 ($Pt_{0.86}Sn_{1.0}P_{1.22}$), PtSnP/C-3 ($Pt_{3.06}Sn_{1.0}P_{2.02}$), PtSn/C-EG ($Pt_{3.10}Sn_{1.0}$), and PtSn/C-B ($Pt_{2.96}Sn_{1.0}$) catalysts, respectively.

Size distributions of the PtSn particles loaded on carbon were evaluated by TEM analysis. Fig. 2 presents the TEM images of (a) PtSnP/C-1, (b) PtSnP/C-2, (c) PtSnP/C-3, (d) PtSn/C-EG and (e) PtSn/C-B catalysts. In Fig. 2a–c, the dark spots of PtSn nanoparticles have a uniform and extremely narrow size distribution with an average diameter of 2 and 1.8 nm, respectively. For the PtSnP/C-1, as noted in Fig. 1a, the image shows a slight increase in the size of the PtSn particles (2–2.2 nm). The PtSn/C-EG and PtSn/C-B catalysts not only have an increment in the size of PtSn nanoparticles (3–5 nm), but also have very poor distribution of the nanoparticles as seen in Fig. 2d and e. The TEM observation demonstrates that the addition of P inhibits the aggregation of PtSn and reduced the size of PtSn nanoparticles, leading higher dispersion of the PtSn nanoparticles with the size distribution of $1.8 \pm 0.5$ nm. It well known that the uniform distribution of the catalysts and a small particle size were key factors for the stable and efficient operation of Direct Methanol (Ethanol) Fuel cells [1–4,39–45]. Daimon et al. [36] and Xue et al. [37] synthesized 2.0 nm of well-dispersed PtRu catalyst nanoparticle supported on carbon, respectively. The about 2 nm of size of PtRu catalysts can simultaneously improve the catalytic activity and utilization efficiency of the catalyst in DMFC application. Therefore, for the fuel cell application, improvement of the catalytic activity and minimization of the Pt requirement will be essential.

Fig. 3 shows the X-ray diffraction (XRD) patterns of (a) PtSnP/C-1, (b) PtSnP/C-2, (c) PtSnP/C-3, (d) PtSn/C-EG and (e) PtSn/C-B electrocatalysts. The first peak at $2\theta$ about 25° was the XC-72 carbon support. It can be seen that both PtSn/C-EG(curve d) and PtSn/C-B (curve e) catalysts display four diffraction peaks of Pt (1 1 1), Pt (2 0 0), Pt (2 2 0) and Pt (3 1 1) at the corresponding diffraction positions, while apart from the four diffraction peaks, there appears diffraction peaks of $SnO_2$ (1 0 1) and $SnO_2$ (2 1 1) at around 34° and 52° (PCPDF#411445) for PtSn/C-EG(curve d) and PtSn/C-B (curve e). The XRD patterns of the PtSnP/C-1, PtSnP/C-2 and PtSnP/C-3 catalysts as shown in Fig. 3B give two broad peak around 34° and 52°. This is assigned to the diffractin peaks of $SnO_2$ (1 0 1) and $SnO_2$ (2 1 1). The XRD diffraction peaks do not contain any distinct peak corresponding to crystalline phase Pt (1 1 1), Pt (2 0 0), Pt (2 2 0) and Pt (3 1 1) for the PtSnP/C-1, PtSnP/C-2 and PtSnP/C-3 catalysts. Three samples all demonstrate amorphous structure,

Table 1
The data from the measurements of EDX, XRD, TEM, etc. for PtSnP/C-1, PtSnP/C-2, PtSnP/C-3, PtSn/C-EG, and PtSn/C-B elecrocatalysts

| | PtSnP/C-1 3:1:30[a] | PtSnP/C-2 3:1:30[a] | PtSnP/C-3 3:1:30[a] | PtSn/C-EG 3:1:0[a] | PtSn/C-B 3:1:0[a] |
|---|---|---|---|---|---|
| Reducing agent | $NaH_2PO_2$ | $NaH_2PO_2$ | $NaH_2PO_2$ $Na_3C_6H_5O_7{\cdot}H_2O$ | Ethanol glycol | $NaBH_4$ |
| Reaction conditions $T$ (°C) | Room temperature | 90 | 90 | 130 | Room temperature |
| Pt:Sn:P at ratio (EDX) | $Pt_{1.57}Sn_{1.0}P_{1.33}$ | $Pt_{0.86}Sn_{1.0}P_{1.22}$ | $Pt_{3.06}Sn_{1.0}P_{2.02}$ | $Pt_{3.10}Sn_{1.0}$ | $Pt_{2.96}Sn_{1.0}$ |
| wt% Pt (bulk) | 6.93 | 7.66 | 14.78 | 15.89 | 16.34 |
| wt% Sn (bulk) | 2.64 | 5.38 | 3.07 | 3.18 | 3.34 |
| wt% P (bulk) | 0.93 | 1.47 | 1.56 | | |
| wt% total (bulk) | 10.50 | 14.52 | 19.41 | 19.07 | 19.68 |
| Average particle size (nm) by TEM | 2.2 | 2 | 1.8 | 3.8 | 3.5 |
| EAS $H_2$ adsorption ($m^2\ g^{-1}$) | – | – | 172 | 123 | 107 |
| EAS CO stripping ($m^2\ g^{-1}$) | – | – | 157 | 94 | 68 |

[a] Pt:Ru:P mole ratios in the mother solution.

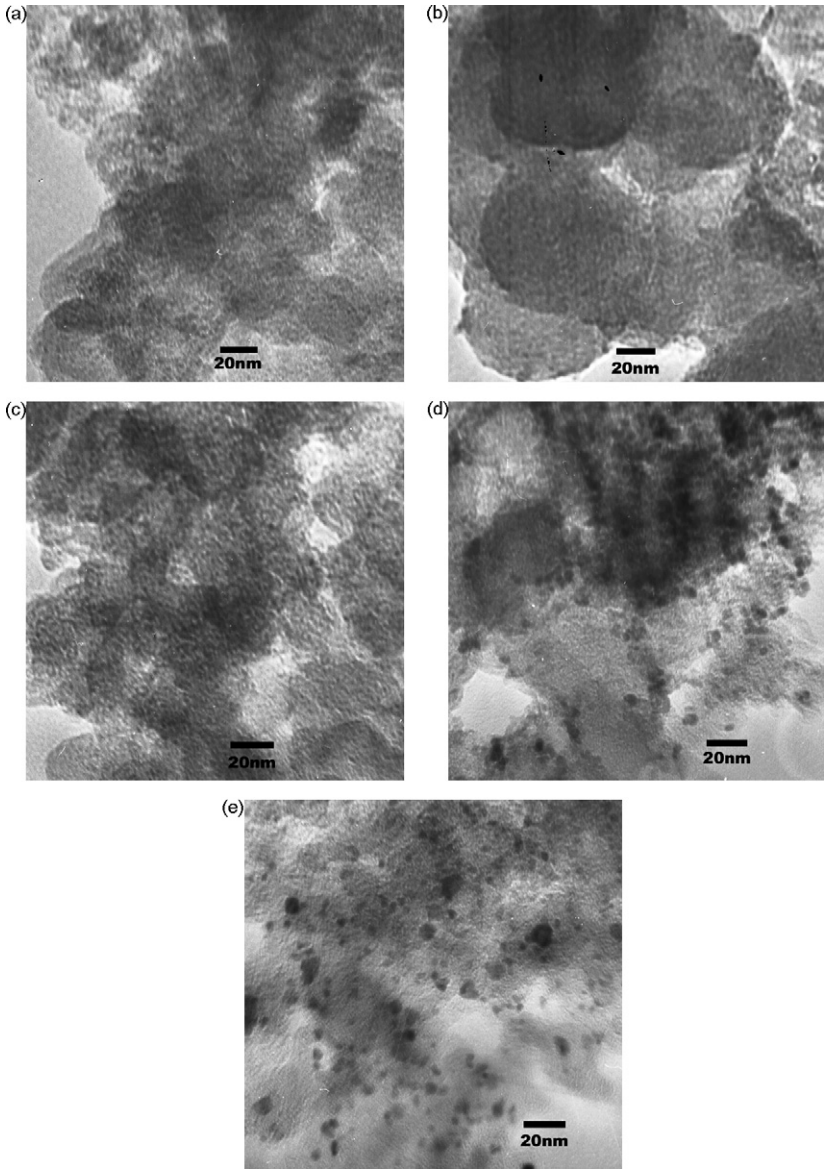


Fig. 2. TEM images of 20 wt% PtSn/C synthesized at different method: (a) PtSnP/C-1, (b) PtSnP/C-2, (c) PtSnP/C-3, (d) PtSn/C-EG and (e) PtSn/C-B electrocatalysts.

which may be attribute to the deposition of phosphorus.In electroless plating of Ni, $NaH_2PO_2$ is known as a reductant, it is well known that P is incorporated into Ni and that Ni becomes amorphous by forming Ni phosphide [29,46,47]. However, two comparatively broad diffraction peaks, located near 43° and 80° $2\theta$, were also present. These peaks do not correspond to the principal diffraction peaks of tin metal.

In Fig. 4(A), we show the Pt 4f spectrum of the PtSnP/C-3, PtSn/C-EG and PtSn/C-B catalysts. The binding energies at the 4f signal for the different 7/2 components were given in Table 2. We find a definite positive shift in the binding energy of Pt 4f for PtSnP/C-3 catalysts in relation to those observed for PtSn/C-EG and PtSn/C-B catalysts. The $4f_{7/2}$ binding energy shifted positively by 1.3 and 2.0 eV for PtSn/C-EG and PtSn/C-B catalysts, respectively. We attribute this effect to an electron transfer involving P, Sn and Pt atoms within the alloy in PtSnP/C-3 catalyst. Since the respective elemental electronegativity values for P,Sn and Pt were 2.52, 1.8 and 2.2, [48,49] respectively. P atoms could produce an electron withdrawing effect from the Pt and Sn atoms bringing about the polarisation of the PtSn bonds in the alloy. In Fig. 4(B), we show the Sn 3d XPS spectrum for PtSnP/C-3, PtSn/C-EG and PtSn/C-B catalysts, The binding energies in various PtSn catalysts as obtained from their XPS spectra were given in Table 2. From these data, we find a slight negative shift in the binding energy of Sn 3d of PtSnP/C-3 for PtSn/C-EG catalyst, while a definite positive shift was observed.

The Chemmical state of P in PtSnP/C-3 catalyst was analyzed by XPS and $P_{2p}$ spectrum was shown in Fig. 4(C). The peaks at the lower and higher binding were assigned to phosphorus interacting with platinum and tin (129.5 eV) and oxidized phosphorus (133.8 eV), respectively. The lower binding energy peak at 129.5 eV shifted negatively by 0.9 eV from that for red phosphorus (130.4). It is concluded that the phosphorus species interacting with platinum and tin were negatively charged and

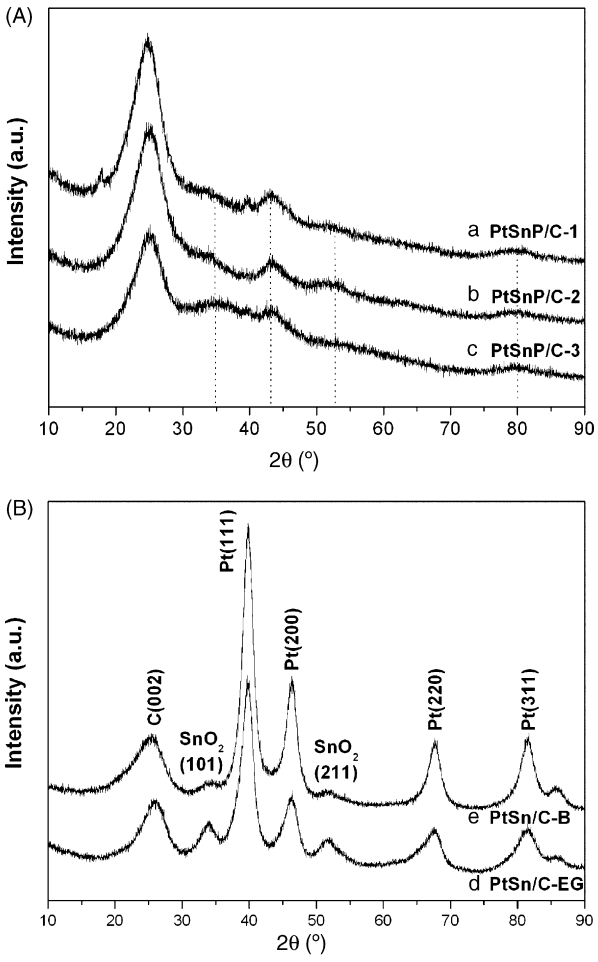


Fig. 3. XRD patterns of (a) PtSnP/C-1, (b) PtSnP/C-2, (c) PtSnP/C-3, (d) PtSn/C-EG and (e) PtSn/C-B electrocatalysts.

that the phosphorus accepts electrons [29,47,48]. There is small peak attributed to pure phosphorus (130.4 eV).

The composition of all samples was evaluate by EDX and provided in Table 1. Fig. 5 shows the typical EDX spectrum of the PtSnP/C-3 catalyst with the nominal atomic composition of $Pt_{3.06}Sn_{1.0}P_{2.02}$. It was found that the P and PtSn coexisted. The XPS and EDX analysis results suggested that P was enriched at the surface of PtSn catalyst nanoparticle. Because of the addition of P and change Pt (1 1 1), Pt (2 0 0) and Pt (2 2 0) plane of the structure of PtSnP catalyst, which was estimated by XRD in Fig. 3(B).Taking these analytical results into account, it is considered that P coexisted with PtSn nanoparticle and that most of P existed in oxidized phosphorus at surface of PtSn catalyst nanoparticle and little forming interstitial compounds.

Fig. 6 shows the cyclic voltammograms of the PtSnP/C-3, PtSn/C-EG and PtSn/C-B catalysts in 0.5 M $H_2SO_4$ electrolytes at room temperature at a scan rate of 10 mV $s^{-1}$ between −0.2 and 0.8 V (versus Ag/AgCl/$Cl^-$). On the three catalysts that well defined hydrogen adsorption/desorption peaks were found. For the PtSnP/C-3 catalyst, well-defined hydrogen adsorption–desorption peaks with a much larger were observed in the potential region −0.2–0.05, demonstrating the higher surface area of the catalyst. The high surface area is owing to the presence of narrow size and uniform distribution of the PtSn nanoparticles as displayed in the TEM (see Fig. 2c). The PtSn/C-EG catalyst exhibits a broad peak relatively with slightly higher current in the adsorption-desorption region than the PtSn/-B catalyst. This is probably due to agglomeration and poor dispersion of the PtSn nanoparticles in these catalysts (see Fig. 2d and e). Electrochemical surface areas of PtSnP/C-3, PtSn/C-EG and PtSn/B electrocatalysts prepared by different methods were 172, 123, and 107 $m^2$ $g^{-1}$ and also listed in Table 1. These values were obtained by calculating the areas under the coulombic charge for hydrogen desorption peaks (see Fig. 6) after subtracting the contribution from double lager charging according to ref 51. It was found that addition P reduces the size of PtSn catalysts nanoparticles and improvement in efficiency of the catalyst caused by the increase the electrochemical surface areas of catalysts.

Fig. 7 shows CO stripping voltammograms of the PtSnP/C-3, PtSn/C-EG and PtSn/C-B catalysts recorded at 10 mV $s^{-1}$ in the 0.5 M $H_2SO_4$ electrolyte at room temperature. The electrochemically active specific surface area of Pt and Sn metals in the Pt–Sn/C catalysts can be calculated from the area of the oxidation peak of $CO_{ad}$ [50]. While electrochemically active specific surface were 157, 94.3, and 68 $m^2$ $g^{-1}$ respectively (as show the Table 1). These data ($EAS_{CO}$) were in good agreement with those of hydrogen desorption ($EAS_{H2}$). The higher activity of PtSnP/C-3 catalysts is attributed to the higher surface area (see Fig. 7 and Table 1). The results of this study further show that the incorporation of P as metalloid elements into the Pt and Sn may act to increase the total surface area. Similar results were obtained by analysis of the Ni–P alloys [51,52,28].

The ethanol cyclic voltammograms results on the five catalysts were shown in Fig. 8. From Fig. 8, it is clear that the addition

Table 2
The performance of single direct ethanol fuel cell of all catalysts

| Catalyst | At room temperature (DEFC) | | | At 70 °C (DEFC) | | |
|---|---|---|---|---|---|---|
| | Open circuit voltage (V) | Maximum power density (mW $cm^{-2}$) | Current density at maximum power density (mA $cm^{-2}$) | Open circuit voltage (V) | Maximum power density (mW $cm^{-2}$) | Current density at maximum power density (mA $cm^{-2}$) |
| PtSnP/C-1 | – | – | – | 0.678 | 36.44 | 150.70 |
| PtSnP/C-2 | – | – | – | 0.671 | 27.42 | 100.10 |
| PtSnP/C-3 | 0.703 | 8.33 | 27.15 | 0.797 | 61.84 | 183.39 |
| PtSn/C-EG | 0.633 | 4.68 | 17.16 | 0.739 | 42.86 | 133.15 |
| PtSn/C-B | 0.574 | 3.97 | 15.15 | 0.747 | 36.52 | 114.13 |

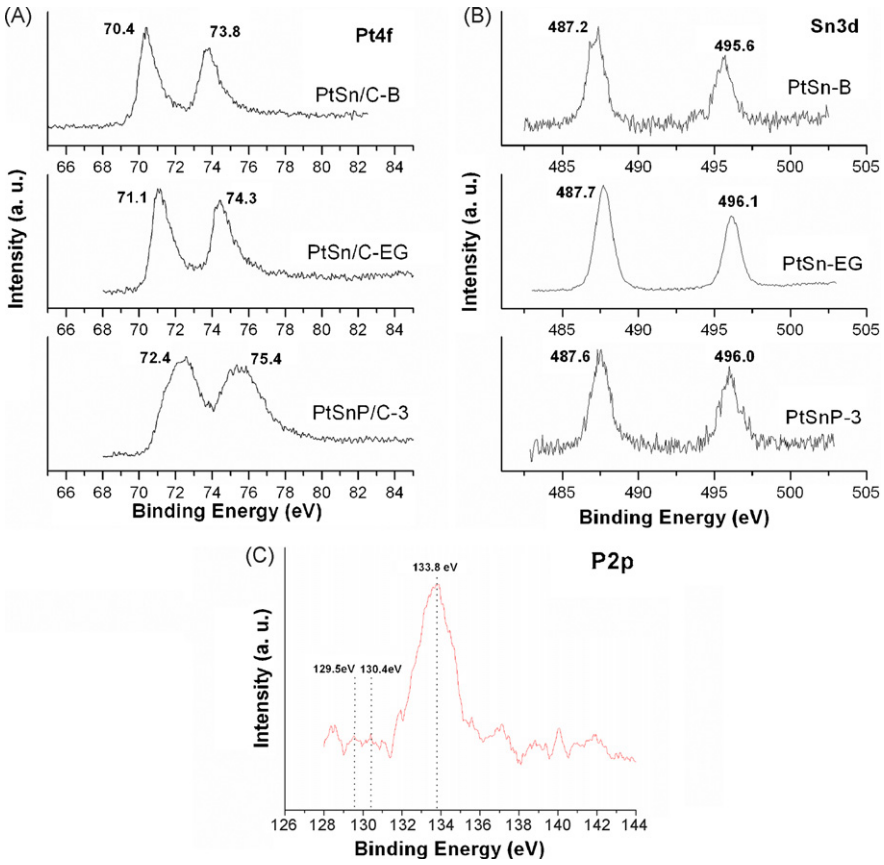


Fig. 4. (A) XPS Spectra for Pt 4f of PtSnP/C-3, PtSn/C-EG and PtSn/C-B electrocatalysts, (B) XPS Spectra for Sn3d of PtSnP/C-3, PtSn/C-EG and PtSn/C-B electrocatalysts.

of the P element to PtSn results in the negative shift of the first ethanol electro-oxidation positive peak. The first positive oxidation peak on PtSnP/C-3 appears at the most negative potential, at about 0.674 V (versus Ag/AgCl/$Cl^-$), and the peak potential is about 0.038 V lower than that on PtSn/C-EG catalyst. The first electro-oxidation peak of ethanol on PtSnPC-1 and PtSnP/C-2 were 0.678 and 0.676 V (versus Ag/AgCl/$Cl^-$), respectively, and lower than that on PtSn/C-B (0.682 V). The PtSnP/C-3 shows the highest positive peak current density and has a lower overpotential (0.674 V versus Ag/AgCl/$Cl^-$). It is clear that the current density is about 1.6 and 2.0 times higher than that PtSn/C-EG and PtSn/C-B catalysts, respectively. The positive current density of ethanol electro-oxidation on PtSnP/C-1 is higher than that on PtSnP/C-2, but less than these on PtSnP/C-3, PtSn/C-EG and PtSn/C-B, respectively. It maybe that the metal content of PtSnP/C-1 and PtSnP/C-2 catalysts is 10.50 and 14.52 wt%, respectively, and lower than these of PtSnP/C-3, PtSn/C-EG and PtSn/C-B catalysts. Therefore, the PtSnP/C-1 and PtSnP/C-2 catalysts show lower activity to ethanol oxidation than other catalysts. From the CV results, it is apparent that the ternary phases

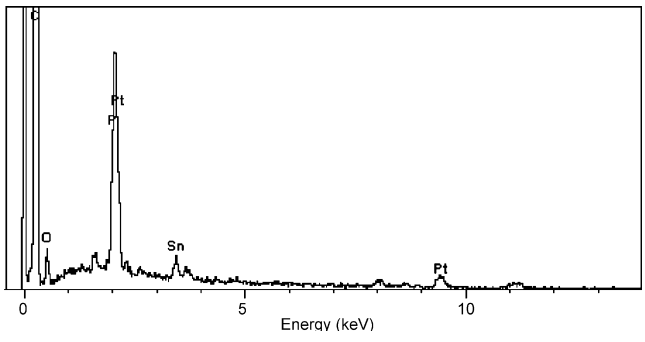


Fig. 5. EDX spectrum of PtSnP/C-3 electrocatalyst.

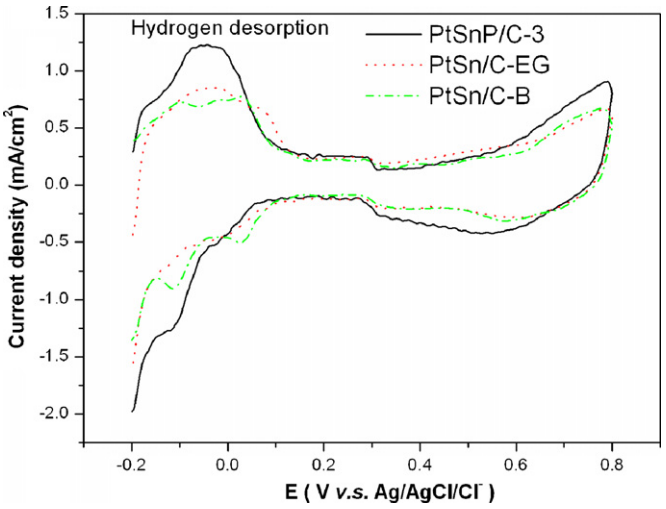


Fig. 6. The cyclic voltammograms of PtSnP/C-3, PtSn/C-EG and PtSn/C-B electrocatalysts in 0.5 M $H_2SO_4$ solution at 10 mV $s^{-1}$ at room temperature.

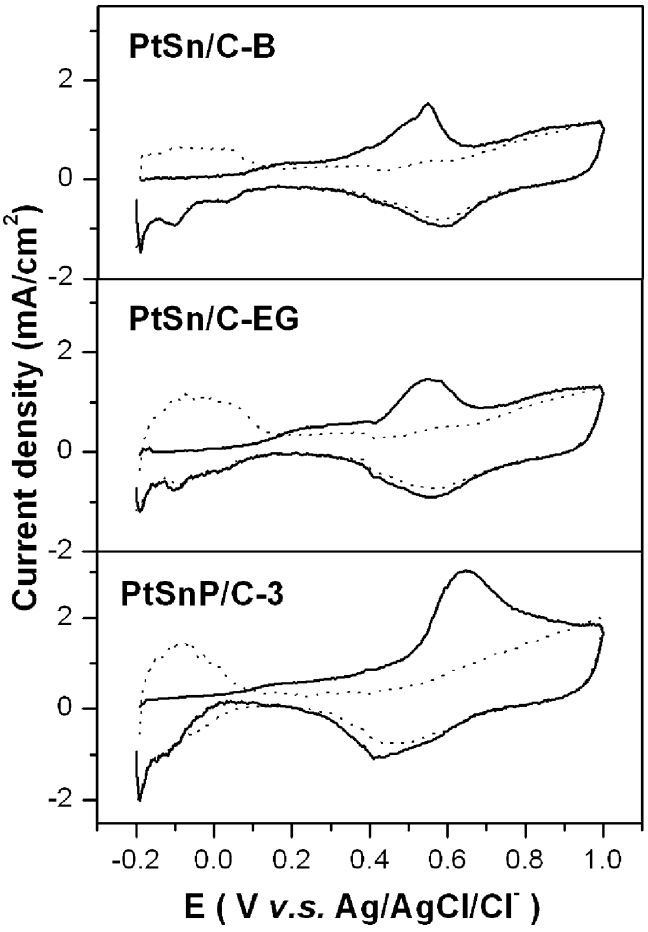


Fig. 7. The $CO_{ad}$ stripping voltammograms of PtSnP/C-3, PtSn/C-EG and PtSn/C-B electrocatalysts in 0.5 M $H_2SO_4$ solution at 10 mV $s^{-1}$ at room temperature.

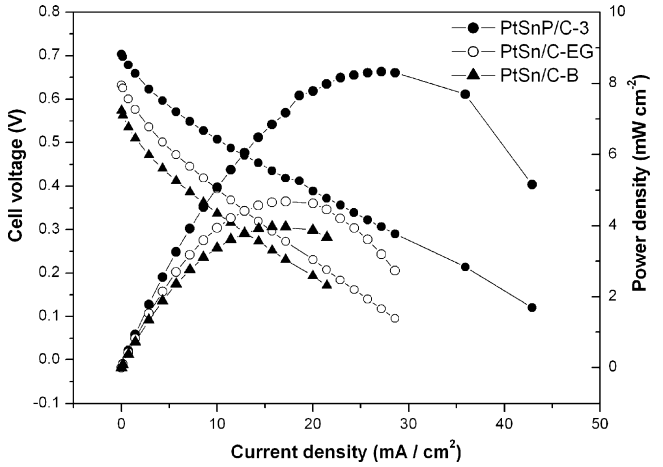


Fig. 9. Voltage as a function of current density for a direct ethanol fuel cell (DEFC) using PtSnP/C-3, PtSn/C-EG and PtSn/C-B as anode electrocatalysts at room temperature.

of composition $Pt_{3.06}Sn_{1.0}P_{2.02}$ (PtSnP/C-3) exhibit higher positive peak current density, and consequently higher activity to ethanol electro-oxidation from the point of current density.

The ethanol oxidation activity of the PtSn/C catalysts was measured with a unit cell. It was well know that at low temperature, the catalysts have a dominating effect on the performance of fuel cells, and comparisons of DEFC performance at relatively low temperature were the most practical and powerful ways of evaluating the activity of catalysts. Fig. 9 shows the performances of single DEFC with PtSnP/C-3, PtSn/C-EG and PtSn/C-B as the anode catalysts at room temperature. The PtSnP/C-3 catalyst shows a current density of 27.25 mA $cm^{-2}$, and exhibits a high maximum power density (8.33 mW $cm^{-2}$) that were 78 and 110% higher than that of the PtSn/C-EG and PtSn/C-B catalysts (4.68 and 3.97 mW $cm^{-2}$). As identified in the CV test, PtSnP/C-3 catalyst shows higher activity than other

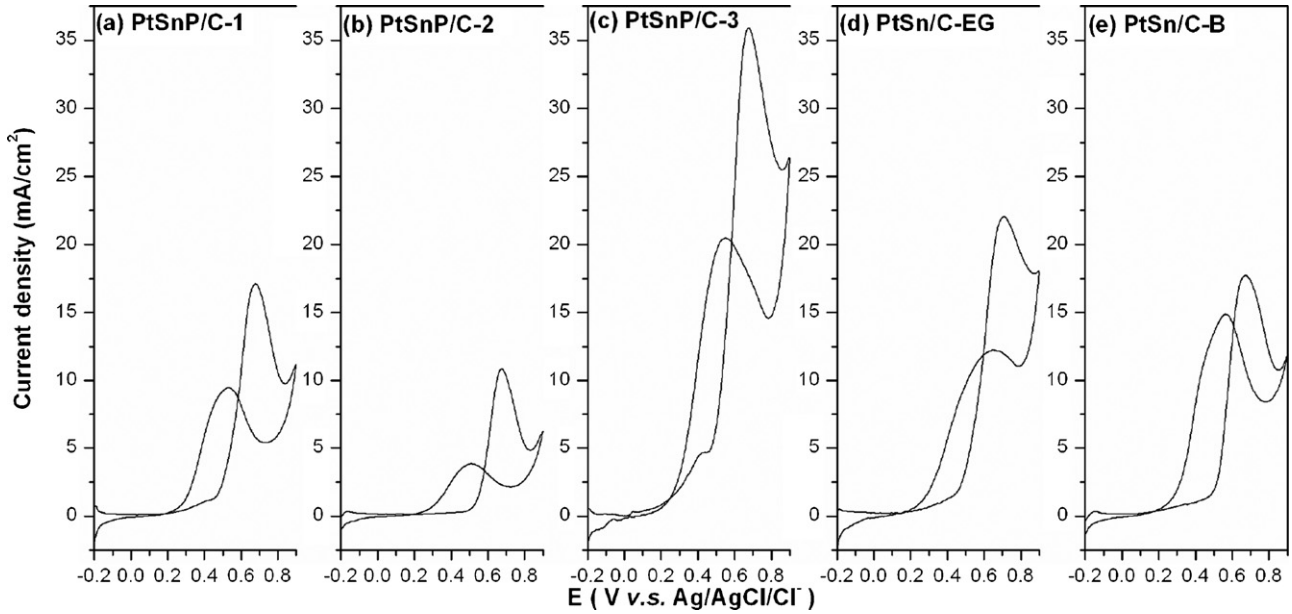


Fig. 8. Cyclic voltammograms of (a) PtSnP/C-1, (b) PtSnP/C-2, (c) PtSnP/C-3, (d) PtSn/C-EG and (e) PtSn/C-B electrocatalysts in 0.5 M $H_2SO_4$ + 1 M $CH_3CH_2OH$ solution at 10 mV $s^{-1}$ at room temperature.

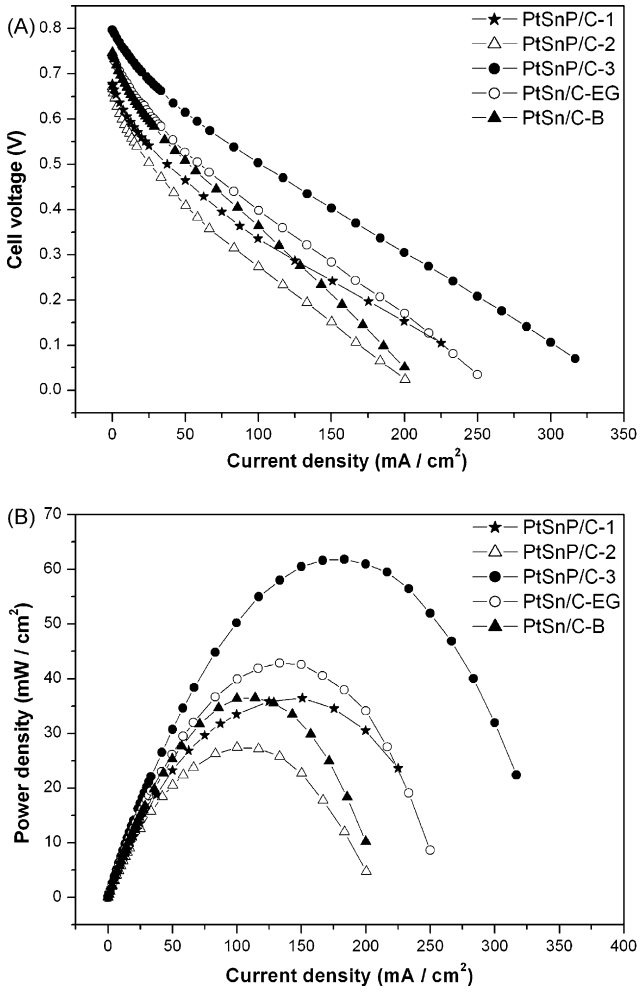


Fig. 10. Voltage (A) and power density (B) as a function of current density for a direct ethanol fuel cell (DEFC) using PtSnP/C-1, PtSnP/C-2, PtSnP/C-3, PtSn/C-EG and PtSn/C-B as anode electrocatalysts at 70 °C.

two catalysts in the single fuel cell tests. The open circuit voltage (OCV) of the single DEFC fuel cell with PtSnP/C-3, PtSn/C-EG and PtSn/C-B as the anode catalysts is 0.703, 0.633 and 0.574 V, respectively. Fig. 10 shows the performances of single DEFC with different anode catalysts at 70 °C.The performance of the single DEFC with PtSnP/C-1 as anode catalyst is similar to that of single DEFC with PtSn/C-B catalyst. The PtSnP/C-3 catalyst produces a higher maximum power density of 61 mW $cm^{-2}$ at 70 °C, which is 150 and 170% higher than that of the PtSn/C-EG and PtSn/C-B catalyst, respectively. Such an improved activity indicates that the addition of P to PtSn enhances the ethanol oxidation activity, and by testing the single DEFC performances. The PtSnP/C-3 ($Pt_{3.06}Sn_{1.0}P_{2.02}$/C) is evidently the more suitable anode catalyst among the five catalyst mentioned above.

## 4. Conclusions

In this paper, the $Pt_3Sn_1$/C and $Pt_3Sn_1P_2$/C catalysts for direct ethanol fuel cell (DEFC) were prepared by using three different methods. We have found that the addition of P reduced the size of PtSn catalyst particle, and to lead to a uniform and extremely narrow size distribution with an average diameter of 2 nm, and to improve the catalytic performance. In contrast to PtSn/C-EG and PtSn/C-B catalysts that prepared by modified polyol method and conventional reduction method, respectively. The electrocatalytic activity of the PtSnP/C-3 ($Pt_3Sn_1P_2$/C) catalysts for the ethanol oxidation was better than that of the PtSn/C-EG and PtSn/C-B catalyst. From combining the results of the electrochemical cell and the practical single DEFC, we conclude that PtSnP/C-3 catalysts was an excellent catalyst for the direct ethanol fuel cell. The PtSnP/C catalyst is hopeful to have a practical application in DMFC.

## Acknowledgments

This work was supported by Science and Technology Ministry of China (863 program Grant No. 2001AA323060, Grant No. 2003AA517060) and the National Natural Science Foundation of China (Grant No. 20373068 and Key Project Grant No. 20433060).

## References

[1] C. Lamy, S. Rousseau, E.M. Belgsir, C. Coutanceau, J.-M. Léger, Electrochim. Acta 49 (2004) 3901.
[2] C. Lamy, E.M. Belgsir, J.-M. Léger, J. Appl. Electrochem. 31 (2001) 799.
[3] J. Wang, S. Wasmus, R.F. Savinell, J. Electrochem. Soc. 142 (1995) 4218.
[4] C. Lamy, A. Lima, V. Le Rhun, F. Delime, C. Coutanceau, J.-M. Léger, J. Power Sources 105 (2002) 283.
[5] E. Peled, T. Duvdevani, A. Aharon, A. Melman, Electrochem. Solid State Lett. 4 (2001) A38.
[6] V.M. Schmidt, R. Ianniello, E. Pastor, S. Gonzalez, J. Phys. Chem. 100 (1996) 17901.
[7] N. Fujiwara, K.A. Friedrich, U. Stimming, J. Electroanal. Chem. 472 (1999) 120.
[8] H. Nonaka, Y. Matsumura, J. Electroanal. Chem. 520 (2002) 101.
[9] H. Hitmi, E.M. Belgsir, J.-M. Léger, C. Lamy, R.O. Lezna, Electrochim. Acta 39 (1994) 407.
[10] T. Iwasita, E. Pastor, Electrochim. Acta 39 (1994) 531.
[11] S.C. Chang, L.W. Leung, M.J. Weaver, J. Phys. Chem. 94 (1990) 6013.
[12] X.H. Xia, H.D. Liess, T. Iwasita, J. Electroanal. Chem. 437 (1997) 233.
[13] J.-M. Léger, J. Appl. Electrochem. 31 (2001) 767.
[14] A. Oliveira Neto, M.J. Giz, J. Perez, E.A. Ticianelli, E.R. Gonzalez, J. Electrochem. Soc. 149 (2002) A272.
[15] F. Delime, J.-M. Léger, C. Lamy, J. Appl. Electrochem. 29 (1999) 1249.
[16] M. Götz, H. Wendt, Electrochim. Acta 43 (1998) 3637.
[17] H. Hitmi, E.M. Belgsir, J.M. Leger, C. Lamy, R.O. Lezna, Electrochim. Acta 39 (1994) 407.
[18] U. Schmiemann, U. Muller, H. Baltruschat, Electrochim. Acta 40 (1994) 99.
[19] D.J. Tarnowski, C. Korzeniewski, J. Phys. Chem. B 101 (1997) 253.
[20] H. Wang, Z. Jusys, R.J. Behm, Fuel Cells 4 (2004) 113.
[21] H. Wang, Z. Jusys, R.J. Behm, J. Phys. Chem. B 108 (2004) 19413.
[22] V.R. Stamenković, M. Arenz, C.A. Lucas, M.E. Gallagher, P.N. Ross, N.M. Marković, J. Am. Chem. Soc. 125 (2003) 2736.
[23] F. Delime, J.-M. Leger, C. Lamy, J. Appl. Electrochem. 28 (1998) 27.
[24] F. Vigier, C. Coutanceau, A. Perrard, E.M. Belgsir, C. Lamy, J. Appl. Electrochem. 34 (2004) 439.
[25] W.J. Zhou, Z.H. Zhou, S.Q. Song, W.Z. Li, G.Q. Sun, P. Tsiakaras, Q. Xin, Appl. Catal. B 46 (2003) 273.
[26] Y. Wang, J. Ren, K. Deng, L. Gui, Y. Tang, Chem. Mater. 12 (2000) 1622.
[27] H. Daimon, O. Kitakami, O. Inagoya, A. Stakemoto, J. Appl. Phys. 30 (1991) 282.
[28] A. Molnar, G.V. Smith, M. Bartok, Adv. Catal. 36 (1989) 329.
[29] Y. Chen, Catal. Today 44 (1998) 3.

[30] J. Deng, J. Yang, S. Sheng, H. Chen, G. Xiong, J. Catal. 150 (1994) 434.
[31] H. Yamashita, T. Funabiki, S. Yoshida, J. Chem. Soc., Faraday Trans. 1 (82) (1986) 1771.
[32] J.V. Wonterghem, S. Morup, J.W. Christion, S. Charles, W.S. Wells, Nature 322 (1986) 622.
[33] G. Luo, S. Yan, M. Qiao, K. Fan, J. Mol. Catal. A: Chemical 230 (2005) 69–77.
[34] Y. Okamoto, Y. Nitta, T. Teranishi, S. Teranishi, J. Chem. Soc., Faraday Trans. 1 (75) (1979) 2027.
[35] W.D. King, J.D. Corn, O.J. Murphy, D.L. Boxall, E.A. Kenik, K.C. Kwiatkowski, S.R. Stock, C.M. Lukehart, J. Phys. Chem. B 107 (2003) 5467.
[36] H. Daimon, Y. Kurobe, Catal. Today 111 (2006) 182.
[37] X. Xue, J. Ge, C. Liu, W. Xing, T. Lu, Communications 8 (2006) 1280–1286.
[38] X.Z. Xue, T.H. Lu, C.P. Liu, Y. Su, Y.Z. Lv, W. Xing, Electrochim. Acta 50 (2005) 3470.
[39] T.S. Ahmadi, Z.L. Wang, T.C. Green, A. Henglein, M.A. El-sayed, Science 272 (1996) 1924.
[40] H. Bönnermann, N. Waldöfner, Chem. Mater. 14 (2002) 1115.
[41] X. Zhang, K.-Y. Chan, Chem. Mater. 15 (2003) 451.
[42] M.S. Nashner, A.I. Frenkel, D. Adler, J.R. Shapley, R.G. Nuzzo, J. Am. Chem. Soc. 119 (1997) 7760.
[43] G. Che, B. Lakeshmi, E. Fisher, C. Martin, Nature 393 (1998) 346.
[44] C. Bock, C. Paquet, M. Couillard, G.A. Botton, B.R. MacDougall, J. Am. Chem. Soc. 126 (2004) 8028.
[45] M.S. Wilson, S. Gottesfeld, J. Appl. Electrochem. 1 (1992) 1.
[46] J.P. Bonino, S. Bruet-Hotellaz, C. Bories, P. Pouderoux, A. Rousset, J. Appl. Electrochem. 27 (1997) 1193.
[47] S.P. Lee, Y.W. Chen, Ind. Eng. Chem. Res. 40 (2001) 1495.
[48] J. Shen, B.E. Spiewak, J.A. Dumesic, Langmuir 13 (1997) 2735.
[49] J.E. Huheey, E.A. Keiter, R.Li. Keiter, Inorganic Chemistry Principles of Structure and Reactivity, 4th ed., Harper Collins College Publishers, New York, 1993.
[50] A. Pozio, M. De Francesco, A. Cemmi, F. Cardellini, L. Giorgi, J. Power Sources 105 (2002) 13.
[51] Y. Okamoto, E. Matsunaga, T. Imanaka, S.J. Teranishi, Catalyst 74 (1982) 183.
[52] S. Yoshida, H. Yamashita, T. Funabiki, T. Yonezawa, J. Chem. Soc., Faraday Trans. 1 (80) (1984) 1435.